Polarization dynamics of a Brillouin fiber ring laser

S. Randoux and J. Zemmouri

*Laboratoire de Physique des Lasers, Atomes et Molécules, Associé au Centre National de la Recherche Scientifique,
Centre d'Etudes et de Recherches Lasers et Applications, Université des Sciences et Technologies de Lille,
F59655 Villeneuve d'Ascq Cedex, France*

The usual three-wave description of stimulated Brillouin scattering (SBS) in birefringent fibers is revised by considering that the pump beam is not necessarily linearly polarized parallel to one of the main axes. The equations obtained govern the dynamics of SBS in a polarization maintaining fiber whatever the state of polarization of the light. A model describing the polarization dynamics of a Brillouin fiber ring laser is then obtained by completing these equations by appropriate boundary conditions. For various orientations of the fiber axes and various polarizations of the incident pump beam, the behaviors of a short-length Brillouin laser are finally studied by numerical simulations that are systematically compared to experimental results. [S1050-2947(99)08302-X]

PACS number(s): 42.65.Es, 42.65.Sf

I. INTRODUCTION

The Brillouin fiber ring laser is a system whose dynamical behavior is now well understood. As long as the input pump power is sufficiently low to avoid the second-order Stokes emission [1] it can exhibit two kinds of operating regimes. The first one is a stationary regime in which a very coherent cw Stokes wave is backscattered by the optical fiber. This steady ''Brillouin mirror'' can be easily obtained if the fiber is short enough [2]. The free spectral range (FSR) of the ring laser is then comparable to the width of the Brillouin gain curve and the Stokes emission involves only one cavity mode. On the other hand, the laser behavior becomes completely different if the cavity FSR is small in comparison to the width of the gain bandwidth. A large number of cavity modes are then able to oscillate and pulsed regimes, associated with a multimode Stokes emission, are observed near the threshold [3]. However, even if the fiber is long, the Brillouin laser generates a stable cw Stokes beam at high enough input pump power [4].

The previously described behaviors are observed for Brillouin lasers made with polarization maintaining fibers. Moreover, the laser ring structure is commonly designed so that the polarization of the optical fields always remains linear. However, recent experiments have shown that the behavior of a short Brillouin fiber laser becomes qualitatively different if the ring structure is slightly modified to scramble the light polarization along the fiber [5]. This was simply achieved by rotating by 90° one of the fiber ends. The slow axis at the input end being then nearly parallel to the fast axis at the output end, the laser no longer operates in the Brillouin mirror regime but exhibits polarization instabilities. Periodic and quasiperiodic regimes have thus been observed and a polarization resolved analysis has revealed an antiphase dynamics between two eigendirections characterizing the laser. Obviously, the theoretical study of such a behavior cannot be undertaken within the framework of the model usually used. One of its major assumption lies indeed in the fact that the polarization of the light beams remains linear all along the fiber. This leads to a well-established model involving two optical waves and an acoustic wave.

In this paper we extend the usual three-wave model of stimulated Brillouin scattering (SBS) by taking into account the fact that the state of polarization (SOP) of the light can change inside the fiber. This is achieved in Sec. II by considering that any optical field can be decomposed with respect to the two orthogonally polarized modes supported by the birefringent fiber. By performing a classical treatment, we obtain equations governing the dynamics of SBS in a polarization maintaining fiber whatever the SOP of light. In Sec. III they are completed by the boundary conditions characterizing a ring laser. This section is also devoted to the study of the static properties of the passive ring resonator. The evolution of the intracavity intensity and the nature of the eigenstates of polarization are thus considered for various orientations of the fiber axes. A normalization of the equations governing the laser dynamics is then performed in Sec. IV. Finally, the laser behavior is studied by numerical simulations that are presented in Sec. V. The obtained results are compared to that already experimentally observed. Furthermore, configurations corresponding to other orientations of the fiber axes and other polarizations of the incident pump beam are also investigated both experimentally and numerically. We conclude in Sec. VI.

II. ESTABLISHMENT OF THE MODEL

One way to deal with polarization effects occurring inside the fiber consists in introducing a depolarization factor. This point of view is often adopted by authors studying the behavior of Brillouin generators or SBS in the presence of weak external feedback. It is based on the fact that the SOP of the output Stokes light can differ from that of the pump laser. The depolarization factor is obtained by measuring the percentage of Stokes power contained in the polarization direction parallel to that of the incident laser. The effective Brillouin gain is then deduced by multiplying the maximum gain by the depolarization factor. Such an approach has been essentially developed for studies of SBS in polarization-scrambled fibers. It leads to results in good agreement with experimental data for the Brillouin generator in which gain narrowing of the Stokes spectrum is observed [6]. Dynamical

aspects in fibers with feedback have also been studied by including a depolarization factor, but SBS was not the only nonlinear effect involved in the interaction [7].

The previously described way to tackle the problem is rather simplified and is inadequate to describe SBS in the highly birefringent fiber used in our laser. In that case, the theoretical treatment of the nonlinear interaction first requires a tensorial analysis of the medium optical properties. Following Ref. [8], the dielectric tensor can be decomposed into the sum of a static part ε_{ik}^0 and of a fluctuating part $\Delta\varepsilon_{ik}$:

$$\varepsilon_{ik} = \varepsilon_{ik}^0 + \Delta\varepsilon_{ik}. \qquad (1)$$

If an appropriate choice of dielectric axes is made, the static part of the tensor takes a simple form and the knowledge of the principal dielectric constants $\varepsilon_{xx}, \varepsilon_{yy}, \varepsilon_{zz}$ is sufficient to describe the static properties of the optical fiber. Light scattering arises from fluctuations in the dielectric characteristics of the fiber that are described by $\Delta\varepsilon_{ik}$. The writing of this last tensor is crucial because it links the SOP of the Stokes field to that of the pump field. To determine the components of $\Delta\varepsilon_{ik}$ let us consider the experiments in which the evolution of the Brillouin gain is measured as a function of the SOP of the pump and Stokes fields. This kind of experiment is commonly performed with a pump-probe arrangement [9]. In the case of polarization maintaining fibers, the measurements show that the maximum gain is reached when the direction of polarization of the pump and probe fields coincides with one of the birefringent axes of the fiber [10]. The direction of polarization of the probe field remaining parallel to the birefringent axis, the Brillouin gain decreases if the polarization of the pump field is rotated. It becomes negligible if the pump and probe fields are perpendicular to each other. The situation is very different if the angle between the birefringent axis and the probe field is equal to 45°. In these conditions, the Brillouin gain is nearly independent of the polarization azimuth of the pump beam and is approximately one-half the maximum gain. Those results have been explained by Stolen [11] and clearly allow us to write

$$\Delta\varepsilon_{ik} = \Delta\varepsilon\,\delta_{ik}, \qquad (2)$$

where $\Delta\varepsilon$ is a scalar and δ_{ik} is the Kronecker symbol. It is then natural to write the electric field as a superposition of the two orthogonally polarized modes able to propagate in the fiber:

$$\mathbf{E}(x,y,z,t) = E_x(x,y,z,t)\mathbf{i} + E_y(x,y,z,t)\mathbf{j}. \qquad (3)$$

In the expression (3) the direction z is the propagation direction. x and y are two transverse directions that are chosen to coincide with the principle axes of the fiber. Those axes are orthogonal and characterized by the refractive indices n_x and n_y. For guided propagation through a single mode optical fiber, the usual treatment consists in ignoring the transverse variation of the electric fields so that we can write

$$E_x(x,y,z,t) = E_x(z,t) = E_{px}(z,t) + E_{sx}(z,t), \qquad (4a)$$

$$E_y(x,y,z,t) = E_y(z,t) = E_{py}(z,t) + E_{sy}(z,t), \qquad (4b)$$

where E_{px} and E_{py} (E_{sx} and E_{sy}) represent the orthogonally polarized pump (Stokes) fields. In the case of SBS, one can consider that each of these fields is composed of a high-frequency carrier modulated by a narrow bandwidth envelope:

$$E_{pl}(z,t) = A_{pl}(z,t)e^{i(\omega_p t - k_{pl}z)} + \text{c.c.} \quad (l=x,y), \qquad (5a)$$

$$E_{sl}(z,t) = A_{sl}(z,t)e^{i(\omega_s t + k_{sl}z)} + \text{c.c.} \quad (l=x,y). \qquad (5b)$$

The envelopes $A_{ml}(z,t)$ ($m=p,s; l=x,y$) of the fields are slowly varying on time scales comparable to the optical period and on distances comparable to the wavelength. ω_p is the pulsation of the pump laser. The pulsation ω_s of the Stokes wave is given by $\omega_s = \omega_p - \omega_a$, where ω_a is the pulsation of the acoustic wave. The propagation of the optical waves inside the fiber is characterized by the wave vectors $k_{ml} = n_l\omega_m/c$ ($m=p,s$ and $l=x,y$), where c is the velocity of light in vacuum.

Following an analogous approach, the acoustic wave created in the interaction can be written as

$$\tilde{\rho}(z,t) = \rho(z,t)e^{i(\omega_a t - k_a z)} + \text{c.c.} \qquad (6)$$

$k_a = \omega_a/c_s$ is the wave vector of the material wave and c_s is its velocity in the fiber. In Eq. (6) the acoustic wave is supposed to be plane. This assumption can be discussed because a fiber, even optically monomodal, can be acoustically multimodal. One of the most spectacular manifestations of this effect is the guided-acoustic-wave Brillouin scattering (GAWBS) [12,13]. Even if recent experiments tend to show a coupling between SBS and GAWBS in a laser [14], we will nevertheless restrict ourselves to the usual approximation that consists in neglecting the influence of transverse effects for the acoustic wave.

The expressions for the acoustic and optical waves now being established, the following step of our theoretical analysis consists in introducing them into the equations coupling their spatiotemporal evolution [Eqs. (8.3.11) and (8.3.16) of Ref. [8]]. By using the slowly varying approximation for phases and amplitudes (SVAPA), we obtain the following set of equations

$$\frac{\partial A_{py}}{\partial t} + \frac{c}{n_y}\frac{\partial A_{py}}{\partial z} + \frac{\gamma_e}{2}A_{py} = iK\rho A_{sy}, \qquad (7a)$$

$$\frac{\partial A_{px}}{\partial t} + \frac{c}{n_x}\frac{\partial A_{px}}{\partial z} + \frac{\gamma_e}{2}A_{px} = iK\rho A_{sx}e^{-i\Delta kz}, \qquad (7b)$$

$$\frac{\partial A_{sy}}{\partial t} - \frac{c}{n_y}\frac{\partial A_{sy}}{\partial z} + \frac{\gamma_e}{2}A_{sy} = iK\rho^* A_{py}, \qquad (7c)$$

$$\frac{\partial A_{sx}}{\partial t} - \frac{c}{n_x}\frac{\partial A_{sx}}{\partial z} + \frac{\gamma_e}{2}A_{sx} = iK\rho^* A_{px}e^{i\Delta kz}, \qquad (7d)$$

$$\frac{\partial\rho}{\partial t} + c_s\frac{\partial\rho}{\partial z} + \gamma_a\rho = iK'(A_{py}A_{sy}^* + A_{px}A_{sx}^*e^{i\Delta kz}), \qquad (7e)$$

where γ_e represents the damping rate of the optical fields. $\gamma_a = \pi\Delta\nu_B$ is the damping coefficient of the acoustic wave and $\Delta\nu_B$ is the full width at half maximum of the Brillouin

gain curve. Rigorously speaking, $K=(\omega_m/2n_l^2)(\partial\varepsilon_{ll}/\partial\rho)(l=x,y$ and $m=p,s)$ is a coupling constant that slightly changes from one equation to the other one. However, the relative amplitude of this change is very low ($\simeq 10^{-4}$) and henceforth we will consider that K is a constant that is given by $K=(\omega/2n)(\partial\varepsilon/\partial\rho)$. $n=(n_x+n_y)/2$ is the average value of the fiber refractive index. ω is equal to $2\pi c/n\lambda$, where λ is the pumping wavelength. The strength of the electrostrictive effect is given by the coefficient $\partial\varepsilon/\partial\rho=p_{12}(n^4/\rho_0)$. p_{12} is the longitudinal elasto-optic coefficient in fused silica and ρ_0 is the average fiber density. Finally, the coupling constant K' of Eq. (7e) is given by $(\varepsilon_0\rho_0\omega_a/4c_s^2)(\partial\varepsilon/\partial\rho)$.

Equations (7) clearly evidence the mechanisms of the interaction occurring inside the fiber. The optical waves polarized along the x and y directions are not coupled to each other as in a cascade process [1], but mutually interact via the same material wave. Let us now explain the origin of the terms $e^{\pm i\Delta kz}$ that appear in the equation governing the dynamics of the acoustic wave [Eq. (7e)] and in the equations involving the optical fields that are polarized along the x direction [Eqs. (7b) and (7d)]. As already mentioned, the Brillouin interaction is submitted to a resonance condition ($\omega_p=\omega_s+\omega_a$). Usually, SBS involves only one of the principle axes of the fiber. If this axis is denoted y, the Brillouin gain is maximized when the phase-matching relation $k_a=k_{py}+k_{sy}$ is precisely verified. By ignoring the x direction, this directly leads to the three-wave SBS model. In our problem, SBS occurs along the two transverse directions and, if we assume that the phase-matching condition $k_a=k_{py}+k_{sy}$ is fulfilled for the y direction, it cannot be the case for the x direction. Along this transverse axis, the phase-matching relation characterizing the interaction reads $k_{px}+k_{sx}=k_a+\Delta k$, where one can easily show that $\Delta k=[(n_x-n_y)/n_x]k_a$. The functions $e^{\pm i\Delta kz}$ appear during the SVAPA and are responsible for a modulation of the source terms related to the x direction. This modulation expresses the fact that the two transverse directions are not characterized by the same Brillouin gain. Let us emphasize that the gain is not necessarily maximum for the y direction and lower for the x direction. This depends on the boundary conditions and an appropriate choice of the phase of the incident fields can lead as well to an opposite situation.

By introducing the variables $\rho_x(z,t)$ and $\rho_y(z,t)$ defined by the relation

$$\rho(z,t)=\rho_y(z,t)+\rho_x(z,t)e^{i\Delta kz} \tag{8}$$

and by neglecting the influence of cross terms appearing on the right-hand side ($\Delta k\simeq 2000$ m^{-1}), we obtain the following set of equations for the description of the interaction:

$$\frac{\partial A_{py}}{\partial t}+\frac{c}{n_y}\frac{\partial A_{py}}{\partial z}+\frac{\gamma_e}{2}A_{py}=iK\rho_yA_{sy}, \tag{9a}$$

$$\frac{\partial A_{px}}{\partial t}+\frac{c}{n_x}\frac{\partial A_{px}}{\partial z}+\frac{\gamma_e}{2}A_{px}=iK\rho_xA_{sx}, \tag{9b}$$

$$\frac{\partial A_{sy}}{\partial t}-\frac{c}{n_y}\frac{\partial A_{sy}}{\partial z}+\frac{\gamma_e}{2}A_{sy}=iK\rho_y^*A_{py}, \tag{9c}$$
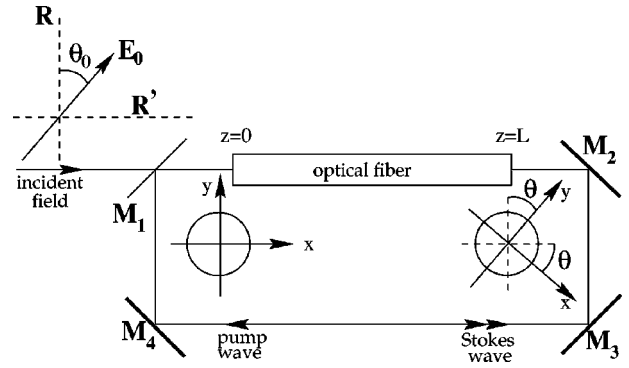

FIG. 1. Schematic representation of the Brillouin fiber ring laser. θ_0 is the angle between the direction of polarization of the incident field $\mathbf{E}_0$ and the y axis. The output end of the fiber is rotated by an angle θ. All the resonator losses are localized on the mirror M_1 characterized by the reflection coefficients R and R'.

$$\frac{\partial A_{sx}}{\partial t}-\frac{c}{n_x}\frac{\partial A_{sx}}{\partial z}+\frac{\gamma_e}{2}A_{sx}=iK\rho_x^*A_{px}, \tag{9d}$$

$$\frac{\partial\rho_y}{\partial t}+c_s\frac{\partial\rho_y}{\partial z}+\gamma_a\rho_y=iK'A_{py}A_{sy}^*, \tag{9e}$$

$$\frac{\partial\rho_x}{\partial t}+c_s\frac{\partial\rho_x}{\partial z}+(\gamma_a+ic_s\Delta k)\rho_x=iK'A_{px}A_{sx}^*. \tag{9f}$$

In these equations, the x direction is decoupled from the y direction. The y-polarized pump wave interacts with the y-polarized Stokes wave through mechanisms described by the usual set of three equations and the same process occurs for the x direction. However, as already explained, the gain is never identical for the two directions because there always exists a frequency detuning equal to $c_s\Delta k$ between the two orthogonally polarized Stokes waves. The writing of Eqs. (9) could let suppose that the y-polarized (x-polarized) optical waves are coupled to a ''y-polarized (x-polarized) acoustic wave.'' To discuss this point of view, let us consider the change of variables given by Eq. (8). Unlike Eq. (3), the decomposition performed in Eq. (8) is not vectorial but shows that the acoustic wave consists of two components, each of them oscillating around a given spatial frequency. The phase-matching relation being precisely verified for the y direction, this spatial frequency is equal to zero for this direction. On the other hand, as the phase-matching condition is not strictly fulfilled for the x direction, the x-polarized optical waves interact with the component ρ_x whose spatial frequency is shifted around Δk.

III. BOUNDARY CONDITIONS, INTRACAVITY INTENSITY, AND EIGENSTATES OF POLARIZATION

From a theoretical point of view, the ring resonator described in Ref. [5] is equivalent to that presented in Fig. 1. M_2, M_3, and M_4 are polarization insensitive mirrors characterized by a reflectivity equal to 1. All the resonator losses are assumed to be localized on the mirror M_1. The anisotropy of these losses is described by a polarization-dependent reflectivity. The reflection coefficient for the amplitude of the fields polarized parallel (perpendicular) to the plane of inci-

dence is denoted R' (R). In our study, the incident pump field $\mathbf{E}_0$ is assumed to be linearly polarized. Its polarization direction forms an angle θ_0 with the y axis at the input end of the fiber. In the general case, the output end of the fiber is rotated by an angle θ so that the boundary conditions characterizing the laser read

$$E_{py}(z=0,t)=E_0(1-R)\cos\theta_0 + R\cos\theta E_{py}(z=L,t)$$
$$-R\sin\theta E_{px}(z=L,t), \qquad (10a)$$

$$E_{px}(z=0,t)=E_0(1-R')\sin\theta_0 + R'\cos\theta E_{px}(z=L,t)$$
$$+R'\sin\theta E_{py}(z=L,t), \qquad (10b)$$

$$R'E_{sx}(z=0,t)=E_{sy}(z=L,t)\sin\theta + E_{sx}(z=L,t)\cos\theta, \qquad (10c)$$

$$RE_{sy}(z=0,t)=E_{sy}(z=L,t)\cos\theta - E_{sx}(z=L,t)\sin\theta. \qquad (10d)$$

The length L of the optical fiber being much greater than that of the optical path separating M_2 from M_1, the delay associated with the corresponding propagation has been neglected in the establishment of Eqs. (10). By setting $E_0 = A_0 e^{i\omega_p t}$ and by using the expressions given by Eqs. (5a) and (5b), the boundary conditions finally read

$$A_{py}(z=0,t)=A_0(1-R)\cos\theta_0 + R\cos\theta A_{py}(z=L,t)e^{-ik_{py}L}$$
$$-R\sin\theta A_{px}(z=L,t)e^{-ik_{px}L}, \qquad (11a)$$

$$A_{px}(z=0,t)=A_0(1-R')\sin\theta_0$$
$$+R'\cos\theta A_{px}(z=L,t)e^{-ik_{px}L}$$
$$+R'\sin\theta A_{py}(z=L,t)e^{-ik_{py}L}, \quad (11b)$$

$$R'A_{sx}(z=0,t)=A_{sy}(z=L,t)\sin\theta e^{ik_{sy}L}$$
$$+A_{sx}(z=L,t)\cos\theta e^{ik_{sx}L}, \qquad (11c)$$

$$RA_{sy}(z=0,t)=A_{sy}(z=L,t)\cos\theta e^{ik_{sy}L}$$
$$-A_{sx}(z=L,t)\sin\theta e^{ik_{sx}L}. \qquad (11d)$$

A_0 is the amplitude of the incident pump field and the frequency detuning parameters $\delta_{ml}=k_{ml}L$ ($m=p,s$ and $l=x,y$) express the fact that the cavity is not necessarily resonant for all the optical waves. It can be easily shown that the frequency detuning parameter δ_{mx} ($m=p,s$) characterizing an x-polarized wave can be linked to the frequency detuning parameter characterizing a y-polarized wave through the relation

$$\delta_{mx}=\delta_{my}\left(1+\frac{n_x-n_y}{n_y}\right) \quad (m=p,s). \qquad (12)$$

At first sight, this seems to show that δ_{mx} is perfectly determined if δ_{my} is known. However, we are going to see that the length and the birefringence of the fiber are not known with an accuracy sufficient to link δ_{mx} to δ_{my} in a simple way. Let us suppose that the cavity length is tuned so that δ_{py} is precisely a multiple of 2π. Mathematically, this can

be written as $\delta_{py}=2\pi j$, where j is an integer equal to $n_y L/\lambda$. The difference between δ_{px} and δ_{py} then reads

$$\delta_{px}-\delta_{py}=2\pi j\frac{n_x-n_y}{n_y}=2\pi\frac{L(n_x-n_y)}{\lambda}. \qquad (13)$$

For values of fiber length, pumping wavelength, and birefringence that are representative of the experiments ($L\simeq 12$ m, $\lambda\simeq 800$ nm, and $n_x-n_y\simeq 10^{-4}$), the term $L(n_x-n_y)/\lambda$ is approximately equal to 1500. In these conditions, we can choose to write $\delta_{px}-\delta_{py}$ as the sum of a multiple of 2π and of a term $\bar{\phi}_p$ comprised between 0 and 2π:

$$\delta_{px}-\delta_{py}=2\pi j'+\bar{\phi}_p. \qquad (14)$$

In practice, the values of L and n_x-n_y are not known with an accuracy better than a few percent. However, even a slight relative variation ($\simeq 10^{-3}$) of the value of one of these parameters leads to a change in the numerical value of $L(n_x-n_y)/\lambda$ that is of the order of unity. Therefore, the parameters j' and $\bar{\phi}_p$ cannot be accurately defined. This is not very important for the term $2\pi j'$ that can be ignored with regard to the boundary conditions. It is more problematic for the value of $\bar{\phi}_p$ that can drastically change if the numerical values of L and n_x-n_y are slightly modified. Obviously, an analogous argumentation can also be developed for the frequency detuning parameters characterizing the Stokes wave. In fact, if one detuning parameter is fixed, the others can be considered as arbitrary. However, if the value of one of them increases by a given quantity, the value of the others increases by the same quantity. Therefore, we will henceforth consider that

$$\delta_{px}=\delta_{py}+\phi_p, \qquad (15a)$$

$$\delta_{sy}=\delta_{py}+\phi_{sy}, \qquad (15b)$$

$$\delta_{sx}=\delta_{py}+\phi_{sx}. \qquad (15c)$$

ϕ_p, ϕ_{sy}, and ϕ_{sx} are arbitrary parameters that are comprised between 0 and 2π. Let us emphasize that, in the experiments, the values of ϕ_p, ϕ_{sy}, and ϕ_{sx} always drift because of slight random changes in the values of L, λ, and n_x-n_y. Rigorously speaking, ϕ_p, ϕ_{sy}, and ϕ_{sx} must be considered as stochastic parameters. However, in the present paper, we are going to assume that they drift sufficiently slowly to be considered as constants during the acquisition time of the temporal signals ($\simeq 0.01$ s). Therefore, in the numerical simulations, the parameters ϕ_p, ϕ_{sy}, and ϕ_{sx} will be considered as time independent and their values will be chosen in order to obtain the best agreement between theory and experiments.

Let us now restrict the problem to the study of the passive ring resonator (i.e., no Brillouin gain $K=K'=0$) operating in time-independent regime. We are first going to establish the general expression giving the evolution of the intracavity pump intensity as a function of the frequency detuning parameter δ_{py}. If we neglect the propagation losses (i.e., $\gamma_e=0$), the fields A_{py} and A_{px} are independent of z and Eqs. (11a) and (11b) become

$$A_{py} = A_0(1-R)\cos\theta_0 + R\cos\theta A_{py}e^{-i\delta_{py}}$$
$$- R\sin\theta A_{px}e^{-i\delta_{px}}, \tag{16a}$$

$$A_{px} = A_0(1-R')\sin\theta_0 + R'\cos\theta A_{px}e^{-i\delta_{px}}$$
$$+ R'\sin\theta A_{py}e^{-i\delta_{py}}. \tag{16b}$$

The resolution of Eqs. (16) allows us to express the normalized intracavity pump fields A_{px}/A_0 and A_{py}/A_0 as functions of R, R', δ_{py}, ϕ_p, θ, and θ_0:

$$\frac{A_{py}}{A_0} = \frac{(1-R)\cos\theta_0 - \dfrac{(1-R')R\sin\theta\sin\theta_0 e^{-i(\delta_{py}+\phi_p)}}{1-R'\cos\theta e^{-i(\delta_{py}+\phi_p)}}}{1-R\cos\theta e^{-i\delta_{py}} + \dfrac{RR'\sin^2\theta e^{-i(2\delta_{py}+\phi_p)}}{1-R'\cos\theta e^{-i(\delta_{py}+\phi_p)}}}, \tag{17a}$$

$$\frac{A_{px}}{A_0} = \frac{(1-R')\sin\theta_0 + R'\sin\theta\dfrac{A_{py}}{A_0}e^{-i\delta_{py}}}{1-R'\cos\theta e^{-i(\delta_{py}+\phi_p)}}. \tag{17b}$$

The x and y directions being orthogonal, the total intensity I_p of the intracavity pump field is simply obtained by adding the intensities I_{px} and I_{py} of the two orthogonal fields

$$I_p(R,R',\theta,\theta_0,\delta_{py},\phi_p) = I_{px} + I_{py} = \left|\frac{A_{px}}{A_0}\right|^2 + \left|\frac{A_{py}}{A_0}\right|^2. \tag{18}$$

The parameters θ, θ_0, and ϕ_p being fixed, it is now possible to plot I_p as a function of δ_{py} for values of the coefficients R and R' that characterize the ring resonators studied in our previous works ($R=0.36$ and $R'=0.42$). As the Stokes intensity directly depends on the pump intensity, the evolution thus obtained is comparable to experimental recordings showing the variation of the total Stokes power when the frequency of the pump laser is slowly swept.

The first configuration that we are going to consider is that in which the fast axis at the input end of the fiber is parallel to the fast axis at the output end (i.e., $\theta=0°$). The characteristics of this kind of resonator have been extensively studied for applications such as gyroscopes [15–19]. In that case, the finesse is usually very high and in most of the papers dealing with the behavior of these systems, the authors follow an approach that consists in using the formalism of Jones vectors. They first calculate the one-round transmission matrix of the light inside the resonator. The transmission of the cavity is then derived by considering the loop by loop evolution of the input Jones vector. This method presents an indisputable advantage: It gives access to the eigenstates of polarization (ESOP) of the ring resonator. An ESOP is a SOP that is defined at an arbitrary point of the fiber and remains unchanged after one round-trip in the cavity. Mathematically, the ESOP are expressed as the eigenvectors of the one-round transmission matrix of the ring resonator. If the polarization maintaining ring resonator is ideal, the fiber axes are perfectly aligned. θ is then strictly equal to $0°$ and the ESOP are simply the two linear polarization states that are fixed by the main axes of the fiber. As
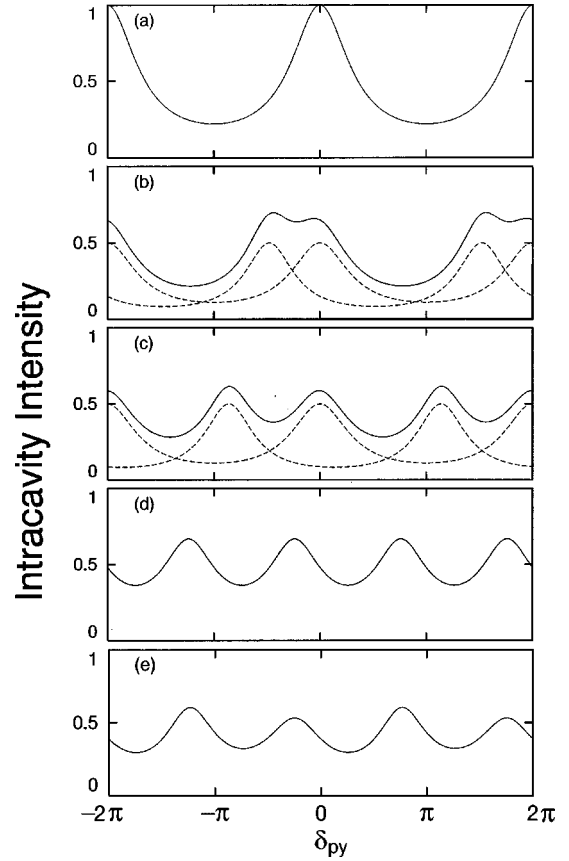

FIG. 2. Evolution of the intracavity intensity as a function of the frequency detuning parameter δ_{py} for various configurations of the resonator ($R=0.36, R'=0.42$). The full lines represent the total intracavity intensity and the dashed lines represent the intensities I_{px} and I_{py} of the orthogonal fields. (a) $\theta=0°, \theta_0=0°$; (b) $\theta=0°, \theta_0=45°, \phi_p=1.5$; (c) $\theta=0°, \theta_0=45°, \phi_p=2.7$; (d) $\theta=90°, \theta_0=0°, \phi_p=1.5$; (e) $\theta=95°, \theta_0=0°, \phi_p=1.5$.

they are orthogonal, the intracavity intensity is the sum of the intensities carried by each ESOP. If $\theta_0=0°$, only one of them is excited and the light remains always linearly polarized along the y axis. The evolution of the intracavity intensity is then simply given by a Airy function ($I_p=I_{py}$) and a resonance is obtained each time that δ_{py} is a multiple of 2π [see Fig. 2(a)]. The frequency detuning parameter δ_{px} does not play any role and the function displayed in Fig. 2(a) is independent of ϕ_p. If $\theta_0=45°$, the two ESOP can be excited and the evolution of the intracavity intensity is completely different from that previously described. As illustrated in Figs. 2(b) and 2(c), the parameter ϕ_p fixes the relative positions of the functions $I_{px}(\delta_{py})$ and $I_{py}(\delta_{py})$. Therefore, its value completely determines the shape of the function $I_p(\delta_{py})$. This behavior will be retrieved in the experiments presented in Sec. V.

The other possibility for an ideal polarization maintaining ring resonator is the configuration in which $\theta=90°$. That kind of resonator has recently been the object of several studies [20,21]. Its two ESOP are the elliptical states of polarization that have been calculated in Ref. [21]. Furthermore, it is now well established that the separation between the resonance frequencies associated with these two ESOP is independent of changes in temperature and is equal to half the FSR. This behavior strongly contrasts with that of the other
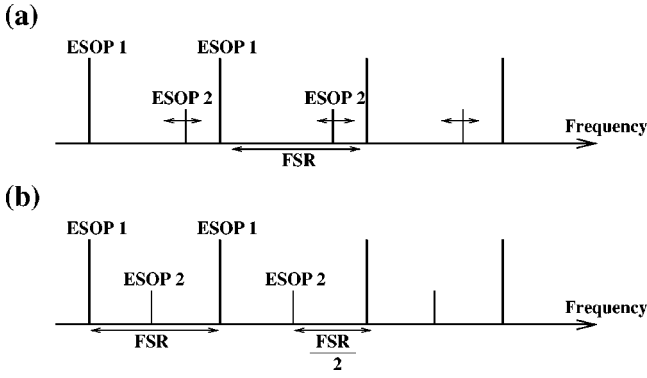
(a)

(b)

FIG. 3. Schematic representation of the resonance characteristics of the Brillouin fiber ring laser. (a) In the usual configuration ($\theta = 0°$), the separation between the resonance frequencies associated with the two orthogonal ESOP drifts if the temperature or the pump wavelength slightly change. (b) In the modified configuration ($\theta = 90°$), the separation between the resonance frequencies associated to the two orthogonal ESOP is immune from temperature or wavelength changes.

resonator ($\theta = 0°$) in which the resonance frequencies associated with the two linear ESOP can cross each other if the temperature (and consequently the birefringence) slightly drifts (see Fig. 3). This immunity from temperature changes can be very useful for technological applications and in particular for Brillouin fiber-optic gyros in which a very stable lasing frequency is required. In the experiments presented in Ref. [5], our ring resonator was pumped with a beam polarized parallel to one of the main axes of the fiber. In this situation, $\theta_0 = 0°$ and the input SOP replicates itself after two round-trips so that the maxima of the intracavity intensity are now periodically spaced of π [Fig. 2(d)]. The maximum intracavity intensity is lower than unity because of the losses occurring on the mirror M_1 at the end of the first round-trip. For this resonator, a change in the value of ϕ_p does not lead to a change in the shape of the function presented in Fig. 2(d), but only induces a global shift in the position of the resonances.

The previous discussion is related to ideal resonators but in a real polarization maintaining ring resonator, there is always a coupling between the ESOP. It comes from a slight misalignment of the fiber axes at the recoupling and it is responsible for the fact that the two ESOP are generally nonorthogonal. For these conditions, the intracavity intensity cannot be written as the sum of the intensities carried by each ESOP and a perturbative cross term expressing the coupling between the two ESOP must be taken into account [18]. However, the nature of the ESOP previously described (for $\theta = 0°$ and $\theta = 90°$) is not fundamentally perturbed as long as the misalignment of the axes is slight. Let us recall that the relations (17) and (18) have been established by considering fields propagating along the x and y axes. As these axes are always orthogonal, these equations are valid whatever the angles θ and θ_0. This is particularly true when the ESOP characterizing the ring resonator are not orthogonal. The relations (17) and (18) can thus be used to study the influence of a misalignment of the main axes on the shape of the function $I_p(\delta_{py})$. Slight variations ($\simeq 10°$) of θ around 90° entails a significant change in this function [see Fig. 2(e)]. Unlike Fig. 2(d), the modulation depth of the intracav-

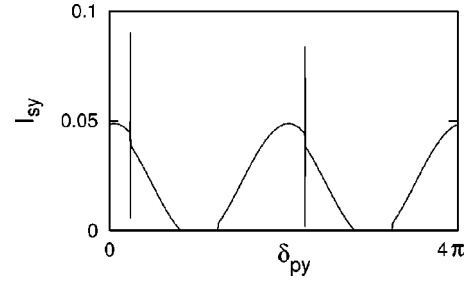FIG. 4. ''Usual'' configuration. Response of the Brillouin laser to a slow sweeping of the frequency detuning parameter $\delta_{py}(\theta = 0°, \theta_0 = 0°, \phi_{sy} = 3.0)$.

ity intensity does not remain constant whatever the values of δ_{py}. That effect has already been observed in the experiments in which the frequency of the pump laser was slowly swept [see Figs. 4(a) and 4(b) of Ref. [5]]. The alignment of the axes was not perfect and the total Stokes power (which directly depends on the intracavity pump power) was found to follow an evolution that was quite similar to that presented in Fig. 2(e). If a slight misalignment of the fiber axes around $\theta = 90°$ leads to an effect that is easily observable, it is not the case for values of θ around 0°. Indeed, numerical simulations show that slight imperfections in the alignment of the axes ($\theta \simeq 10°$) do not alter significantly the function I_p presented in Fig. 2(a). This is confirmed by the experiments performed in the configuration of the ''usual'' Brillouin laser. In that case, the accuracy of the alignment of the axes was not better than a few degrees, but the modulation depth of the intracavity intensity was constant [see Fig. 2(b) of Ref. [5]].

IV. NORMALIZATION

Equations (9) govern the dynamics of SBS in a birefringent fiber. They consist of two independent sets of three equations. The first one is the usual three-wave model describing the interaction of a y-polarized pump wave with a y-polarized Stokes wave. The second set involves x-polarized optical waves that experience a gain slightly different from that of the y direction. In the two sets of equations, the velocities of the optical waves slightly differ. This allows us to introduce two time scales on which the variable t is normalized with respect to the times taken by the light to propagate inside the fiber along the two axes:

$$\tau = \frac{ct}{n_y L}, \qquad \tau' = \frac{ct}{n_x L}. \qquad (19)$$

Obviously, these time scales are not independent and if τ is fixed, τ' is given by

$$\tau' = \left(1 + \frac{n_y - n_x}{n_x}\right)\tau. \qquad (20)$$

By writing the spatial coordinate z in units of fiber length

$$\zeta = \frac{z}{L} \qquad (21)$$

and by considering that the y- (x-) polarized waves now become functions of τ (τ') and ζ, the velocities of the x-

and y-polarized waves are thus normalized to unity. The theoretical and numerical analyses of the model are also facilitated by the introduction of dimensionless amplitudes. If A_{max} is the maximum amplitude that can be reached by the incident pump field, we can first define a dimensionless pump parameter μ by the relation $A_0 = \mu A_{max}$. The dimensionless amplitudes ε_{ml} of the optical fields are then obtained after a normalization with respect to A_{max}:

$$\varepsilon_{ml} = \frac{A_{ml}}{A_{max}} \quad (m=p,s; l=x,y). \tag{22}$$

The amplitudes of the acoustic waves can be rescaled in the form

$$B_l = \frac{-i\gamma_a}{A_{max}^2 K'}\rho_l \quad (l=x,y). \tag{23}$$

With these new variables, Eqs. (9) become:

$$\frac{\partial \varepsilon_{py}}{\partial \tau} + \frac{\partial \varepsilon_{py}}{\partial \zeta} + \frac{\beta}{2}\varepsilon_{py} = -gB_y\varepsilon_{sy}, \tag{24a}$$

$$\frac{\partial \varepsilon_{px}}{\partial \tau'} + \frac{\partial \varepsilon_{px}}{\partial \zeta} + \frac{\beta}{2}\varepsilon_{px} = -gB_x\varepsilon_{sx}, \tag{24b}$$

$$\frac{\partial \varepsilon_{sy}}{\partial \tau} - \frac{\partial \varepsilon_{sy}}{\partial \zeta} + \frac{\beta}{2}\varepsilon_{sy} = gB_y^*\varepsilon_{py}, \tag{24c}$$

$$\frac{\partial \varepsilon_{sx}}{\partial \tau'} - \frac{\partial \varepsilon_{sx}}{\partial \zeta} + \frac{\beta}{2}\varepsilon_{sx} = gB_x^*\varepsilon_{px}, \tag{24d}$$

$$\frac{1}{\beta_A}\frac{\partial B_y}{\partial \tau} + B_y = \varepsilon_{py}\varepsilon_{sy}^*, \tag{24e}$$

$$\frac{1}{\beta_A}\frac{\partial B_x}{\partial \tau'} + (1+i\Delta)B_x = \varepsilon_{px}\varepsilon_{sx}^*, \tag{24f}$$

where $\beta = \gamma_e nL/c$, $\beta_A = \gamma_a nL/c$, $\Delta = c_s\Delta k/\gamma_a$, and $g = KK'nLA_{max}^2/\gamma_a c$. The velocity of the sound being much lower than that of the light, the term corresponding to the propagation of the acoustic wave has been neglected in the establishment of Eqs. (24e) and (24f). In the ring laser, the x and y directions are coupled by boundary conditions that take the normalized form

$$\varepsilon_{py}(\zeta=0,\tau) = \mu(1-R)\cos\theta_0 + R\cos\theta\varepsilon_{py}(\zeta=1,\tau)e^{-i\delta_{py}}$$
$$-R\sin\theta\varepsilon_{px}(\zeta=1,\tau')e^{-i(\delta_{py}+\phi_p)}, \tag{25a}$$

$$\varepsilon_{px}(\zeta=0,\tau') = \mu(1-R')\sin\theta_0 + R'\cos\theta\varepsilon_{px}(\zeta=1,\tau')$$
$$\times e^{-i(\delta_{py}+\phi_p)} + R'\sin\theta\varepsilon_{py}(\zeta=1,\tau)e^{-i\delta_{py}}, \tag{25b}$$

$$R'\varepsilon_{sx}(\zeta=0,\tau') = \varepsilon_{sy}(\zeta=1,\tau)\sin\theta e^{i(\delta_{py}+\phi_{sy})}$$
$$+\varepsilon_{sx}(\zeta=1,\tau')\cos\theta e^{i(\delta_{py}+\phi_{sx})}, \tag{25c}$$

$$R\varepsilon_{sy}(\zeta=0,\tau) = \varepsilon_{sy}(\zeta=1,\tau)\cos\theta e^{i(\delta_{py}+\phi_{sy})}$$
$$-\varepsilon_{sx}(\zeta=1,\tau')\sin\theta e^{i(\delta_{py}+\phi_{sx})}. \tag{25d}$$

Henceforth, Eqs. (24) and (25) will be our working equations. They govern the dynamics of a Brillouin ring laser made with a polarization maintaining fiber and they generalize the usual three-wave model by including additional degrees of freedom associated with the polarization of the fields. The following section is devoted to a comparison between the experimentally observed behaviors and the results obtained by the numerical integration of these equations.

V. GENERAL FEATURES OF THE LASER BEHAVIOR

The physical data used to compute the reduced parameters appearing in Eqs. (24) and (25) are those commonly found in SBS literature [22]: p_{12}, c_s, and ρ_0 are, respectively, equal to 0.286, 5.96×10^3 m s^{-1}, 2.21×10^3 kg m^{-3}. The other parameters characterize the ring laser used in our experiments. The fiber is 12 m long and its core diameter is equal to 2.75 μm. At the working wavelength of 800 nm, the average value n of its refractive index is 1.45. Furthermore, the birefringence $n_x - n_y$ of the fiber is equal to 10^{-4} and its absorption coefficient is 1.2×10^{-3}m^{-1}. The width $\Delta\nu_B$ of the gain curve is estimated to 60 MHz and the Brillouin shift is $\omega_a = 2\pi\times(20\times10^9)$ s^{-1}. Finally, the maximum power available to pump the Brillouin laser is 1 W. The corresponding amplitude A_{max} of the incident field is then 9.35 MV/m. The values of the reduced parameters used in our study are $g=45.92$, $\beta_A=10.93$, $\beta=0.01$, and $\Delta=0.04$. Let us note that, except for g, these values are identical to those used in Ref. [1]. The difference between the values of the parameter g arises from the choice made for the normalization of the fields. In Ref. [1] the fields were normalized to the maximum electric field launched in the fiber (3.36 MV/m corresponding to a maximum injected power of 0.13 W). In the present paper they are normalized to the maximum electric field available to pump the laser.

Sections V A and V B are respectively devoted to the study of the behavior of the Brillouin laser operating in the usual configuration ($\theta\simeq0°$) and in the "modified" configuration in which $\theta\simeq90°$. Intermediate situations corresponding to other values of the angle θ will be investigated in Sec. V C. Let us recall that the experiments already presented in Ref. [5] have clearly evidenced the importance of the role played by the frequency detuning parameters. In particular, they have shown that an overview of the system dynamics can be obtained by slowly sweeping the frequency of the pump laser. Therefore, in our numerical simulations, we are going to follow an analogous approach and we are going to record the response of the laser to a slow sweeping of δ_{py}. We will consider the evolution of the following dynamical variables: the intensity $I_{sx} = |\varepsilon_{sx}(\zeta=0,\tau)|^2$ of the x-polarized Stokes component, the intensity $I_{sy} = |\varepsilon_{sy}(\zeta=0,\tau)|^2$ of the y-polarized Stokes component and the total Stokes intensity $I_s = I_{sx} + I_{sy}$.

A. Behavior of the laser in the usual configuration ($\theta\simeq0°$)

If the incident pump beam is linearly polarized along the y axis ($\theta_0=0°$), only the y direction is relevant and the model then simply reduces to the three-wave model. In numerical simulations, the Stokes intensity obviously follows an evolution that is similar to that experimentally observed
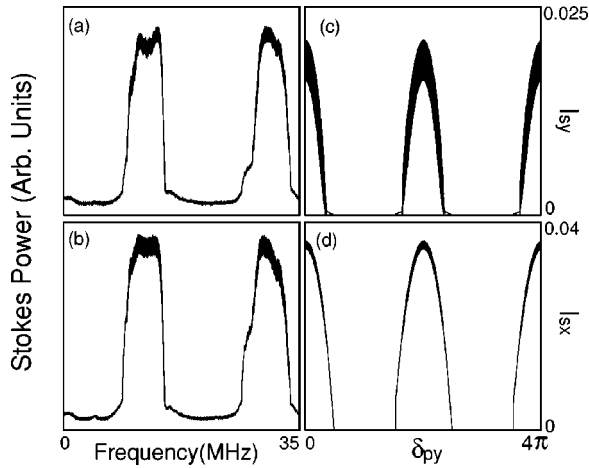
FIG. 5. Usual configuration. Response of the Brillouin fiber ring laser to a slow sweeping of the frequency of the pump laser. (a) and (b) experiments (c) and (d) numerical simulations ($\theta=3°$, $\theta_0=45°$, $\mu=0.197$, $\phi_p=1.0$, $\phi_{sy}=0.5$, $\phi_{sx}=0.0$).
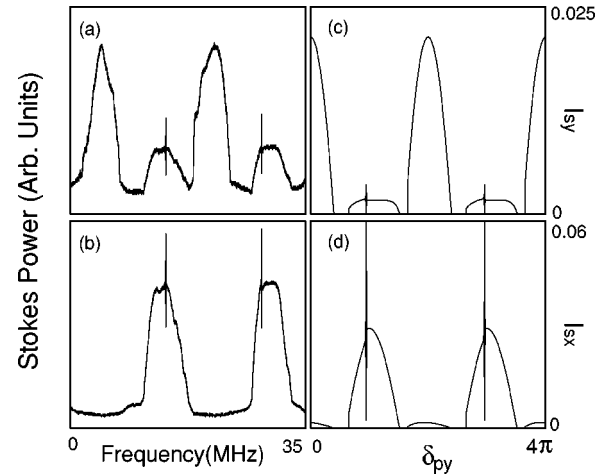

FIG. 6. Usual configuration. Response of the Brillouin fiber ring laser to a slow sweeping of the frequency of the pump laser. (a) and (b) Experiments (c) and (d) numerical simulations ($\theta=10°$, $\theta_0=45°$, $\mu=0.197$, $\phi_p=3.0$, $\phi_{sy}=6.0$, $\phi_{sx}=0.0$).

[see Fig. 2(a) of Ref. [5] and Fig. 4]. Note that slight changes in the orientation of the output end of the fiber ($\theta\simeq10°$) or in the polarization of the input field ($\theta_0\simeq10°$) only induce the emergence of a weak Stokes component polarized along the x direction. Its appearance does not alter significantly the evolution presented in Fig. 4.

Let us now consider the situation in which the direction of polarization of the incident pump beam is rotated so that $\theta_0=45°$. This is experimentally achieved by using the experimental setup described in Ref. [5]. Let us recall that it includes a detection part allowing a polarization resolved analysis of the Stokes light. For this experiment, it was only modified by inserting a half-wave plate between the pump laser and the Brillouin laser. Unlike the situation previously discussed ($\theta_0\simeq0°$), the two ESOP characterizing the ring resonator can now be simultaneously excited. When the frequency of the pump laser is slowly swept, the Brillouin laser then emits simultaneously along the two polarization directions and oscillations of weak amplitude are recorded above the threshold [see Figs. 5(a) and 5(b)]. For appropriate values of the detuning parameters ϕ_p, ϕ_{sx}, and ϕ_{sy}, numerical simulations reveal a behavior that is similar to that experimentally observed [see Figs. 5(c) and 5(d)]. Another kind of situation can also be experimentally observed. If the wavelength of the pump laser is slightly changed ($\simeq0.05$ nm), the two ESOP can now be alternately excited. When the frequency of the pump laser is slowly swept, the Brillouin laser first emits a Stokes wave that is linearly polarized along the y direction. A further increase in the frequency of the pump laser leads to the emission of a Stokes wave presenting a strong component polarized along the x direction and a weak component polarized along the y direction [see Figs. 6(a) and 6(b)]. It is worth noticing that, except when mode hops occurs, the Stokes intensity always remains stable. That kind of behavior is also retrieved in numerical simulations [see Figs. 6(c) and 6(d)] performed for an angle θ equal to $10°$. If the value of θ is taken to $0°$, the numerical simulations show that the Brillouin laser operates on either the y direction or the x direction but never simultaneously on the two directions (i.e., the weak y component disappears).

As long as the value of θ is sufficiently low ($\theta<10°$), the coupling between the x and y directions is weak. One can consider that two Brillouin lasers operate nearly independently along the two transverse directions. As illustrated in Fig. 6, one of them can be above the threshold, whereas the other one is below the threshold. The Stokes intensity is then always stable. On the other hand, both of them can emit simultaneously and unstable behaviors arising from a beating between the two lasing frequencies are observed. The frequency of this beating is of the order of a few megahertz in the experiments and in the numerical simulations. This value is comparable to the width of the resonator resonances.

B. Behavior of the laser in the modified configuration ($\theta\simeq90°$)

In the modified configuration studied in Ref. [5], the fast axis at the input end becomes nearly parallel to the slow axis at the output end ($\theta\simeq90°$) and the input field is linearly polarized along one of these axes ($\theta_0\simeq0°$). By adjusting the values of the parameters μ, ϕ_p, ϕ_{sx}, and ϕ_{sy} it is possible to reproduce global evolutions that are qualitatively similar to that reported in Ref. [5]. As in the experiments, the laser can thus emit a Stokes beam whose intensity is stable for almost all the values of δ_{py} [see Fig. 7(a)]. For higher values of the pump parameter μ, unstable behaviors can also be observed for appropriate values of the detuning parameters [see Fig. 7(b)]. The instabilities revealed by the numerical simulations are of the same nature as that experimentally recorded. They consist of periodic oscillations whose period is approximately equal to 2 in the reduced units adopted for the normalization (see Fig. 8). This means that they are correlated to an effect involving a double round-trip of the light inside the cavity. Moreover, the antiphase motion between the directions x and y is also retrieved in the numerical results. Its existence can be explained in a simple way if we first assume that θ and θ_0 are respectively strictly equal to $90°$ and $0°$. If the values of the pump and detuning parameters are appropriate, a Stokes pulse can grow inside the fiber and propagate along one of the main axes. If that axis is the
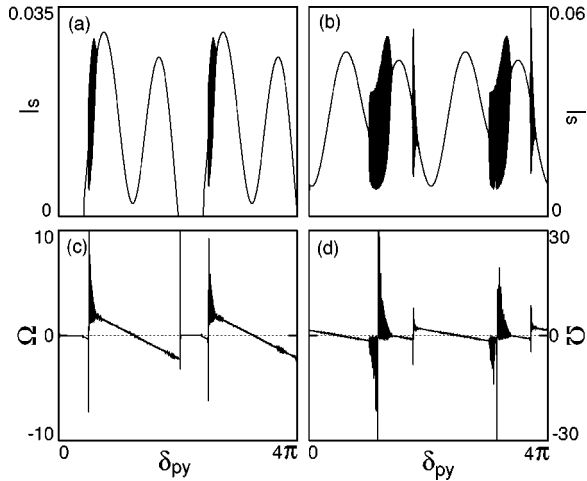
FIG. 7. Modified configuration. (a) and (b) Response of the Brillouin fiber ring laser to a slow sweeping of the frequency detuning parameter δ_{py} and (c) and (d) corresponding evolution of the instantaneous frequency Ω of the y-polarized Stokes wave. The numerical values of the parameters are (a) and (c) $\mu = 0.197, \phi_p = 4.9, \phi_{sy} = 0.3, \phi_{sx} = 0.8, \theta = 100°, \theta_0 = 0°$ and (b) and (d) $\mu = 0.228, \phi_p = 5.9, \phi_{sy} = 0.3, \phi_{sx} = 0.0, \theta = 100°, \theta_0 = 0°$.

y axis, the pulse is first recorded by the detector associated with the y direction. It is then recoupled along the x axis and after one round-trip it is detected by the photodiode associated with the x direction. After a new round-trip along the y axis, it is again detected by the other photodiode. Therefore, the pulse is alternately observed in the y direction and in the x direction. It experiences losses at each recoupling, but these losses are compensated for by the gain acquired during the propagation. The previous argumentation has been formulated for waves that are linearly polarized. However, it remains valid even if the values of θ and θ_0 are not strictly equal to 90° and 0°. Indeed, in these conditions, the SOP of the optical waves is not fundamentally perturbed and one can consider that they remain nearly linearly polarized.

Let us now provide a modal explanation of the behaviors presented in Figs. 7(a) and 7(b). As already discussed in Ref.
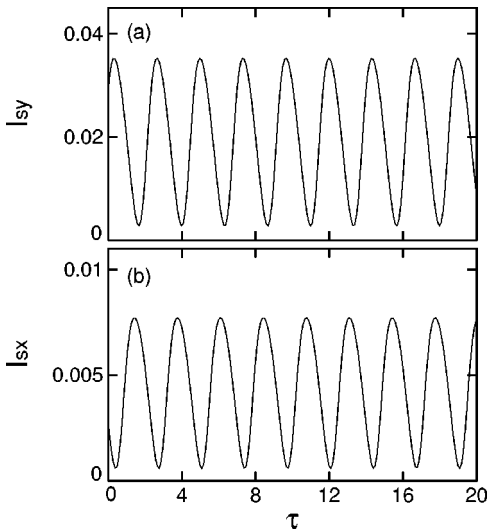

FIG. 8. Modified configuration. Periodic instabilities and antiphase response of the Brillouin fiber ring laser ($\mu = 0.228, \delta_{py} = 3.2, \phi_p = 5.9, \phi_{sy} = 0.3, \phi_{sx} = 0.0, \theta = 100°, \theta_0 = 0°$).

[2], a sweeping of the frequency of the pump laser entails two main effects: a periodic modulation of the intracavity pump power and a displacement of the center of the Brillouin gain curve with respect to the resonance frequencies of the cavity. As the former effect has already been discussed in Sec. III, we will consider only the latter one. When the center of the gain curve is displaced with respect to the resonance frequencies, one can observe situations in which mode hops appear with a periodicity of 2π (17 MHz in the experiments). This is characterized by the appearance of instabilities in the total intensity of the Stokes wave [see Fig. 7(a)]. A way to check that these instabilities are definitely linked to mode hops consists in following the evolution of the instantaneous frequency of the Stokes wave. By writing $\varepsilon_{sy}(\zeta = 0, \tau)$ as $a_{sy}(\zeta = 0, \tau)e^{i\psi_{sy}(\zeta = 0, \tau)}$ and by following the evolution of the variable $\Omega = d\psi_{sy}(\zeta = 0, \tau)/d\tau$ during the sweeping of δ_{py}, one observes discontinuities, allowing one to confirm that the instabilities can be imputed to mode hops [see Fig. 7(c)]. The fact that they appear with a periodicity of 2π shows that the Stokes emission involves only one ESOP and that the other one does not play any role [see Fig. 3(b)]. When wide ranges of instabilities are recorded [Fig. 7(b)], the ESOP1 and ESOP2 of Fig. 3(b) have the same Brillouin gain. The observed instabilities then result from a mode hop from the ESOP1 to the ESOP2. Another mode hop from the ESOP2 to the ESOP1 immediately follows the first one. The fact that it occupies a narrow range of frequencies indicates that the ESOP1 tends to supplant the ESOP2 in the studied laser. This is confirmed in Fig. 7(d), where one can check that, during the sweeping of δ_{py}, the Stokes emission preferentially involves one ESOP.

C. Other configurations ($0° < \theta < 90°$)

Our aim in this section is not to provide a complete description of the laser behaviors. The parameters characterizing the system (μ, θ, θ_0, ϕ_p, ϕ_{sx}, and ϕ_{sy}) are indeed too numerous. For an angle θ_0 close to 0°, we are only going to consider the results of experiments in which the angle θ takes values in the range 0°–90°. In all the situations that have been experimentally studied ($\theta \approx 30°-50°-70°$), the laser rather exhibits a stable behavior with mode hops separated by a FSR ($\simeq 17$ MHz). This is illustrated in Figs. 9(a) and 9(b) for a particular case corresponding to an angle θ approximately equal to 30°. Let us finally note that for that kind of configuration ($0° < \theta < 90°$), numerical simulations reproduce also correctly the experimental behaviors [see, Figs. 9(c) and 9(d)].

VI. CONCLUSION

The polarization dynamics of a Brillouin fiber ring laser has been studied both experimentally and theoretically. The usual description of SBS in birefringent fibers has first been revised by considering that the pump beam is not necessarily polarized parallel to one of the main axes. The adopted approach consists in considering that the optical fields can be decomposed with respect to the two orthogonally polarized modes supported by the fiber. The equations then derived generalize the three-wave model by including additional degrees of freedom associated with the polarization. By com-
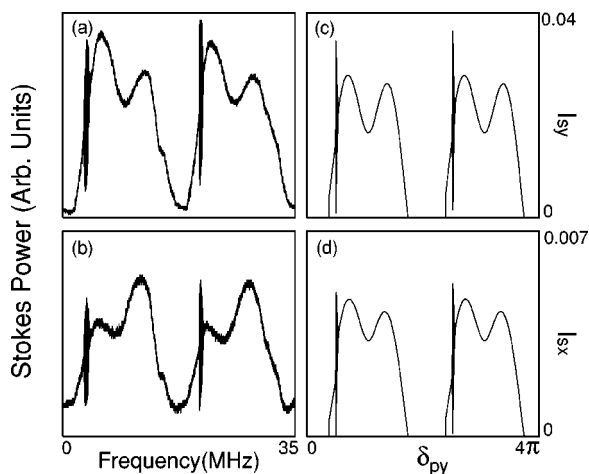
FIG. 9. Response of the Brillouin fiber ring laser to a slow sweeping of the frequency of the pump laser. (a) and (b) Experiments (c) and (d) numerical simulations ($\mu=0.197, \theta=30°, \theta_0=0°, \phi_p=6.0, \delta_{sy}=0.3, \delta_{sx}=0.8$).

pleting them with appropriate boundary conditions, we have obtained a model describing the polarization dynamics of a Brillouin fiber ring laser. The system behavior has then been studied by numerical simulations that have revealed results qualitatively similar to that experimentally observed in various configurations (i.e., for various orientations of the fiber axes and various orientations of the polarization of the incident pump beam).

SBS is the only nonlinear effect that has been taken into account in the establishment of our model, but another nonlinear effect prone to influencing the system dynamics is the optical Kerr effect. The relevance of the inclusion of that kind of nonlinearity in models describing SBS in fibers is a subject that was extensively discussed a few years ago

[6,7,23]. The polemic was essentially related to SBS dynamics in long fibers with or without external feedback. For realistic values of the physical parameters (and in particular the n_2 Kerr coefficient), it has been shown that the ratio of the Kerr to Brillouin nonlinearities is around 0.015 [6]. Even in long fibers, the Kerr effect remains always perturbative so that models incorporating only a Brillouin nonlinearity are very often sufficient to describe correctly the dynamics of the studied systems. In our particular case, the laser dynamics is properly described by a model involving only the Brillouin effect even when the input pump power is sufficiently high to induce the emergence of a second order Stokes component [1]. These considerations associated with the fact that our experimental and theoretical results are in good qualitative agreement confidently allow us to neglect the Kerr effect in the establishment of the model.

From a theoretical point of view, an analytical study of the laser steady states could now be envisaged within the framework of the model previously established. It could lead to interesting results concerning the threshold conditions for the growth of the x- and y-polarized Stokes waves. Furthermore, our numerical and experimental study is related to the behavior of short-length Brillouin fiber lasers. For longer lasers much more longitudinal modes can compete for gain and one can reasonably expect a richer dynamics (eventually presenting chaos). However, that kind of conjecture requires further experimental and numerical studies.

[1] S. Randoux, V. Lecoeuche, B. Ségard, and J. Zemmouri, Phys. Rev. A **52**, 2327 (1995).

[2] S. Randoux, V. Lecoeuche, B. Ségard, and J. Zemmouri, Phys. Rev. A **51**, R4345 (1995).

[3] I. Bar-Joseph, A. Dienes, A. A. Friesem, E. Lichtman, R. G. Waarts, and H. H. Yaffe, Opt. Commun. **59**, 296 (1986).

[4] C. Montes, A. Mamhoud, and E. Picholle, Phys. Rev. A **49**, 1344 (1994).

[5] S. Randoux, V. Lecoeuche, and J. Zemmouri, Phys. Rev. A **56**, R1717 (1997).

[6] A. L. Gaeta and R. W. Boyd, Phys. Rev. A **44**, 3205 (1991).

[7] D. Yu, W. Lu, and R. G. Harrison, Phys. Rev. A **51**, 669 (1995).

[8] R. W. Boyd, *Nonlinear Optics* (Academic, San Diego, 1992).

[9] M. O. van Deventer and A. J. Boot, J. Lightwave Technol. **12**, 585 (1994).

[10] T. Horiguchi, M. Tateda, N. Shibata, and Y. Azuma, Opt. Lett. **14**, 329 (1989).

[11] R. H. Stolen, IEEE J. Quantum Electron. **QE-15**, 1157 (1979).

[12] R. M. Shelby, M. D. Levenson, and P. W. Bayer, Phys. Rev. Lett. **54**, 939 (1985).

[13] R. M. Shelby, M. D. Levenson, and P. W. Bayer, Phys. Rev. B **31**, 5244 (1985).

[14] E. Picholle and A. Picozzi, Opt. Commun. **135**, 327 (1997).

[15] K. Iwatsuki, K. Hotate, and M. Higashiguchi, Appl. Opt. **25**, 2606 (1986).

[16] P. Mouroulis, Appl. Opt. **31**, 2025 (1992).

[17] Z. K. Ioannidis, R. Kadiwar, and I. P. Giles, Opt. Lett. **14**, 520 (1989).

[18] Z. K. Ioannidis, R. Kadiwar, and I. P. Giles, J. Lightwave Technol. **3**, 377 (1996).

[19] B. Lamouroux, B. Prade, and A. Orszag, Opt. Lett. **7**, 391 (1982).

[20] Y. Tanaka and K. Hotate, IEEE Photonics Technol. Lett. **7**, 482 (1995).

[21] K. Hotate and Y. Tanaka, J. Lightwave Technol. **13**, 384 (1995).

[22] J. Botineau, C. Leycuras, C. Montes, and E. Picholle, J. Opt. Soc. Am. B **6**, 300 (1989).

[23] M. Dämmig, G. Zinner, F. Mitschke, and H. Welling, Phys. Rev. A **48**, 3301 (1993).